Biochemistry

© Copyright 1995 by the American Chemical Society Volume 34, Number 43 October 31, 1995

Accelerated Publications

Crystallographic Analysis of Reversible Metal Binding Observed in a Mutant (Asp153 → Gly) of *Escherichia coli* Alkaline Phosphatase‡

Chris G. Dealwis,§ Catherine Brennan,§ Kris Christianson,§ Wlodek Mandecki,§ and Cele Abad-Zapatero*,||

Laboratory of Protein Crystallography, D-46Y, AP10, L-07, Abbott Laboratories, 100 Abbott Park Road, Abbott Park, Illinois 60064-3500, and Viral Discovery, D90D, Building R1, Room 2056, Abbott Laboratories, 1401 Sheridan Road, North Chicago, Illinois 60064-4000

Received June 23, 1995; Revised Manuscript Received September 1, 1995⊗

ABSTRACT: Here we present the refined crystal structures of three different conformational states of the Asp153 → Gly mutant (D153G) of alkaline phosphatase (AP), a metalloenzyme from *Escherichia coli*. The apo state is induced in the crystal over a 3 month period by metal depletion of the holoenzyme crystals. Subsequently, the metals are reintroduced in the crystalline state in a time-dependent reversible manner without physically damaging the crystals. Two structural intermediates of the holo form based on data from a 2 week (intermediate I) and a 2 month soak (intermediate II) of the apo crystals with Mg^{2+} and Zn^{2+} have been identified. The three-dimensional crystal structures of the apo (R = 18.1%), intermediate I (R = 19.5%), and intermediate II (R = 19.9%) of the D153G enzyme have been refined and the corresponding structures analyzed and compared. Large conformational changes that extend from the mutant active site to surface loops, located 20 Å away, are observed in the apo structure with respect to the holo structure. The structure of intermediate I shows the recovery of the entire enzyme to an almost native-like conformation, with the exception of residues Asp 51 and Asp 369 in the active site and the surface loop (406−410) which remains partially disordered. In the three-dimensional structure of intermediate II, both Asp 51 and Asp 369 are essentially in a native-like conformation, but the main chain of residues 406−408 within the loop is still not fully ordered. The D153G mutant protein exhibits weak, reversible, time dependent metal binding in solution and in the crystalline state. In contrast, the wild-type AP binds the metals tightly.

The ability to experimentally observe structural intermediates in biological macromolecules provides a basis for understanding their dynamic processes. Several groups have investigated intermediate species involved in the mechanism of enzyme catalysis (Bartunik, 1983; Hajdu et al., 1987; Schlichting et al., 1990, 1994; Moffat et al., 1992; Teng et al., 1994), protein folding (Moffatt et al., 1986), and calcium release (Hajdu et al., 1988) using a combination of monochromatic and Laue X-ray diffraction. Here we report the crystal structure of three conformational states of the mutant D153G of *Escherichia coli* alkaline phophatase (AP) based on monochromatic data collected using a conventional X-ray source. These structures demonstrate reversible, time dependent metal binding in the crystalline state. Corroborative evidence is also presented of similar behavior of this mutant in solution.

‡ The refined coordinates of the apo, holo, intermediate I, and intermediate II have been deposited in the Brookhaven Protein Data Bank with accession codes 1AJA, 1AJB, 1AJC, and 1AJD, respectively. Until their release, requests should be sent to the corresponding author.

* To whom correspondence should be addressed.
§ Viral Discovery, Abbott Laboratories.
|| Laboratory of Protein Crystallography, Abbott Laboratories.

⊗ Abstract published in *Advance ACS Abstracts,* October 15, 1995.

0006-2960/95/0434-13967$09.00/0 © 1995 American Chemical Society

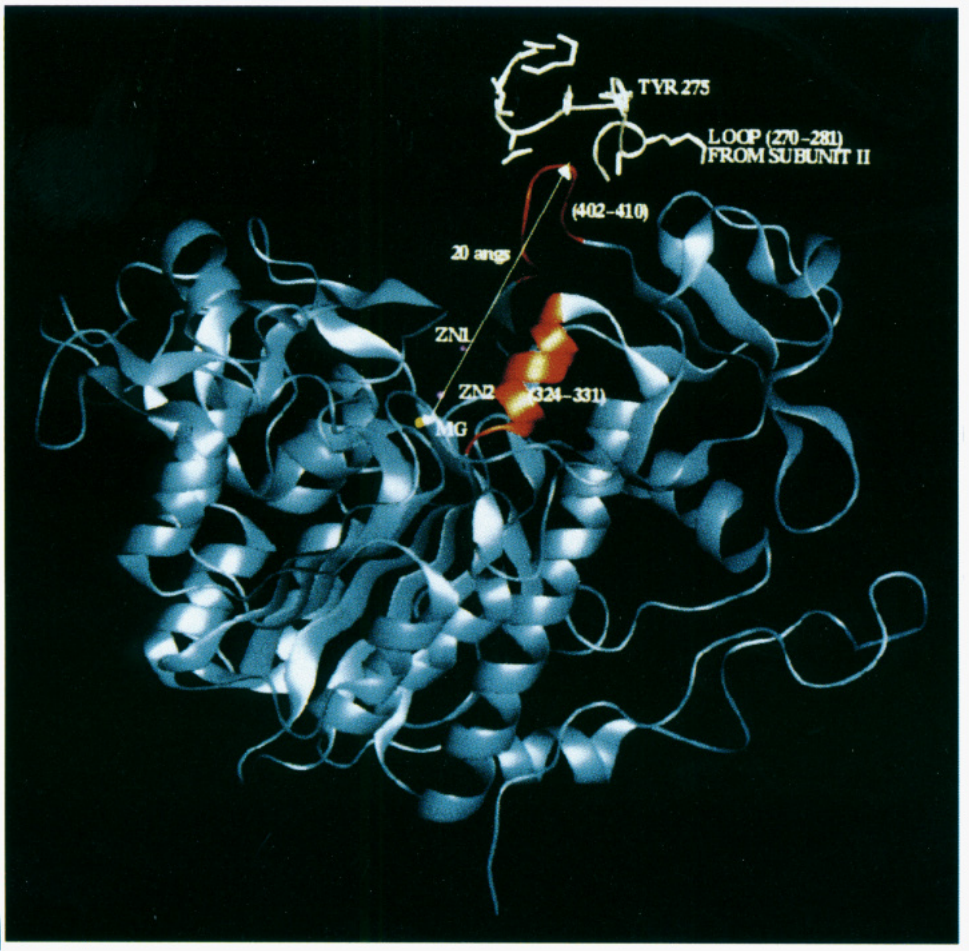

FIGURE 1: Schematic representation of the fold of the D153G mutant AP monomer. Regions undergoing conformational changes due to metal depletion are drawn in red, while the rest of the enzyme is drawn in blue. In order to show that loop 402−410 is at the dimer interface, its contact loop (270−281) from subunit II of the dimer is drawn in white. The arrow drawn in white shows a 20 Å distance taken from the magnesium binding site to the 402−410 loop.

E. coli AP is a dimeric, nonspecific monophosphoesterase (Wilson et al., 1964; Schwartz et al., 1963; Hull et al., 1976; Chlebowski et al., 1977) consisting of 449 amino acid residues and two zinc ions and one magnesium ion per monomer (Figure 1). The active site of AP has been well characterized by site-directed mutagenesis (Gosh et al., 1986; Butler-Ransohoff et al., 1988; Chaidarogou et al., 1988; Chaidaroglou & Kantrowitz, 1989; Mandecki et al., 1991; Matlin et al., 1992; Murphy & Kantrowitz, 1994; Xu et al., 1994), X-ray crystallography (Sowadski et al., 1983; Kim & Wyckoff, 1991; Chen et al., 1992; Murphy et al., 1993; Dealwis et al., 1995), and NMR (Coleman & Gettings 1983). Mutation of the active site residue Asp 153 to alanine, glycine, or histidine has produced mutants with increased activity and decreased magnesium affinity (Matlin et al., 1992; Dealwis et al., 1995; Murphy et al., 1993). Furthermore, relative to the wild-type enzyme, both the D153H and the double mutant D153H/K328H undergo a time-dependent activation induced by Mg^{2+}, which has been suggested to be caused by a conformational change (Janeway et al., 1993). The refined three-dimensional structure of the holoenzyme of the D153G mutant has been reported elsewhere (Dealwis et al., 1995). In this study we report the observation of reversible metal binding of the above mutant in both the crystalline and solution states in a time-dependent manner and the refined crystal structures of the apoenzyme and two conformational states of its holoenzyme.

MATERIALS AND METHODS

The mutant enzyme was prepared as described previously (Dealwis et al., 1995). Crystals of the mutant D153G were obtained using the hanging drop vapor diffusion method described by Chen et al. (1992). If left undisturbed in their drops, the crystals lose their metals after about 3 months, and the apoenzyme crystals are stable in a harvesting solution containing 65% saturated ammonium sulfate and 100 mM Tris-HCl. These crystals did not appear to be damaged and were isomorphous with the wild-type AP crystals (Sowadski et al., 1983) and had cell constants of a =195.02 Å, b =166.93 Å, and c = 76.44 Å in the $I222$ space group with two monomers in the asymmetric unit. Several apoenzyme crystals were placed in a harvesting solution containing 65% saturated ammonium sulfate, 100 mM Tris-HCl, 10 mM zinc chloride, and 10 mM magnesium sulfate, and one was mounted on a quartz capillary tube after 2 weeks of soaking; a second one was mounted after 2 months. These crystals were physically robust and diffracted well to approximately 2.7 Å resolution, in spite of the buffer transfer. X-ray diffraction data were collected at room temperature of the apoenzyme (data set D153GDM), and the two separate crystals were soaked for 2 weeks (D153GX2) and 2 months (D153GX4) in the harvesting solution. We used the oscillation method using a Rigaku RU200 rotating anode as an X-ray source and a Rigaku RAXIS-IIC image plate system equipped with a graphite monochromator for data collection.

Table 1: Data Collection and Refinement Statistics[a]

data set	D153GDM	D153GX2	D153GX4
reflections	65477	25993	24115
R_{sym} (%)	8.0	10.3	12.7[b]
resolution (Å)	2.0	2.8	2.7
completion (%)	76.5	82.2	74.3
final *R*-factor (%)	18.1	19.5	19.9
non-hydrogen protein atoms	6280[c]	6600	6600
metal ions	6	6	6
water molecules	209	220	222
RMS deviation from ideality			
bond lengths (Å)	0.013	0.014	0.014
bond angles (deg)	2.2	2.3	2.4
dihedral angles (deg)	24.2	24.8	24.7
improper dihedral angles (deg)	1.1	1.3	1.4

[a] D153GDM, structure of the D153G mutant determined with data from the apo crystals. D153GX2, intermediate I structure of the D153G mutant determined with data from apo crystals after a 2 week soak of Mg^{2+} and Zn^{2+}. D153GX4, intermediate II structure of the D153G mutant determined with data from apo crystals after a 2 month soak of Mg^{2+} and Zn^{2+}. [b] This data set was collected from a small (approximately 0.100 × 0.100 × 0.05 mm) crystal. [c] Atoms in disordered regions were not included in the refinement.

The typical data collection time was approximately 25 h per data set. The three structures of the D153G mutant based on the data sets D153GDM, D153GX2, and D153GX4 were determined using the refined protein coordinates of the holoenzyme of the same mutant determined using data collected from freshly grown crystals (Dealwis et al., 1995). Initial $F_o - F_c$ difference Fourier maps were computed after several rounds of rigid-body (RB) refinement using the program X-PLOR (Brünger et al., 1987, 1989) and inspected using the program FRODO (Jones, 1978). Finally, all three structures were subjected to several rounds of conjugate gradient refinement interspersed with model building, which included the addition of solvent molecules. Table 1 contains a summary of the merging statistics of the X-ray data and the refinement statistics of the three structures.

In order to obtain approximate relative occupancies of the Mg^{2+} and Zn^{2+} ions at the three metal sites, the electron density (ρ) was calculated at each site using the three data sets D153GNP [holoenzyme from Dealwis et al. (1995)], D153GX2, and D153GX4. First, the structure factor amplitudes of the three data sets were placed in a common scale using the program SCALEIT (Collaborative Computational Project, Number 4, 1994). The electron density was calculated with 20−2.8 Å data for each of the scaled data sets using the refined phases of their respective models based on the protein main-chain and side-chain atoms only. The individual values of ρ were derived by summing over a 1 Å cube about each refined metal ion coordinate at 0.1 Å intervals. These values are not on an absolute scale of electrons/Å^3 but rather on a relative scale using the electron density at the M3 site after 2 weeks' soak as reference (data set D153GX2).

Dialysis was performed at 4 °C using a Pierce Microdialyzer 500 with an 8000 molecular weight cutoff membrane. The AP proteins, wild type, D153G, and D101S, were dialyzed versus 50 mM Tris-HCl, pH 8.1, containing 1 mM EDTA for 24−48 h. Aliquots of the EDTA-dialyzed proteins were then dialyzed in 50 mM Tris-HCl, pH 8.1, containing 10 mM $MgCl_2$ and 1 mM $ZnCl_2$ and aliquots removed at various times and assayed for enzyme activity. The removal and reintroduction of Zn^{2+} and Mg^{2+} metals from the active site of the proteins were assessed by measuring the loss and reactivation of enzyme activity. Enzyme activity was assayed at 5 nM AP protein in 50 mM Tris-HCl, 0.1 mg/mL BSA, and 2 mM *p*-nitrophenyl phosphate (PNPP), pH 8.0, using a Bio-Rad Model 3550 microplate reader as described (Brennan et al., 1994).

Table 2: Individual Relative Electron Density Values and Thermal Parameters of the Metal Ions and Metal···Ligand Distances of the Zn^{2+} and Mg^{2+} Ions in the AP D153G Mutant Structures[a]

	Part a D153GNP (holo)	D153GX2 (int I)	D153GX4 (int II)
rel electron density (ρ)			
M1 Zn^{2+}	3.6	2.0	3.1
M2 Zn^{2+}	3.6	2.4	3.7
M3 Mg^{2+}	1.3	1.0	1.9
B-factor			
M1 Zn^{2+}	10.6	29.0	11.9
M2 Zn^{2+}	14.0	28.0	11.0
M3 Mg^{2+}	15.5	23.6	10.8

	Part b distance (Å)		
metal···ligand	D153GNP (holo)	D153GX2 (int I)	D153GX4 (int II)
M1 site			
Zn^{2+}···OD1 Asp 327	2.1	2.1	2.3
Zn^{2+}···OD2 Asp 327	2.2	2.2	2.2
Zn^{2+}···NE2 His 331	2.2	2.2	2.2
Zn^{2+}···NE2 His 412	2.2	2.0	2.0
M2 site			
Zn^{2+}···OD1 Asp 51	2.2	2.9	2.3
Zn^{2+}···OG Ser 102	2.1	2.1	2.1
Zn^{2+}···OD1 Asp 369	2.2	2.0	2.1
Zn^{2+}···NE2 His 370	2.3	2.3	2.1
M3 site			
Mg^{2+}···O W454	2.5		
Mg^{2+}···O W455	2.5	2.7	2.5
Mg^{2+}···O W456	2.2	2.2	2.2
Mg^{2+}···OD1 Asp 51		2.1	
Mg^{2+}···OD2 Asp 51	2.0		2.1
Mg^{2+}···OG1 Thr 155	2.6	2.9	2.6
Mg^{2+}···OE2 Glu 322	1.9	2.1	2.1

[a] See Table 1 for definitions. All distances, electron density values, and thermal parameters are averaged over both AP subunits. The relative electron density values are expressed as fractions of the value obtained for the Mg^{2+} ion of the D153GX2 data set. See the Materials and Methods section for the procedure used for calculating ρ.

RESULTS AND DISCUSSION

The final *R*-factors of the three conformational states of the D153G AP mutant based on the data sets D153GDM, D153GX2, and D153GX4 (see Materials and Methods for definition) after refinement were 18.1%, 19.5%, and 19.9% and their estimated coordinate error derived from Luzzati plots (Luzzati, 1953) were 0.19 Å, 0.20 Å, and 0.21 Å, respectively. The $F_o - F_c$ electron density map calculated with the rigid-body refined phases showed that the D153GDM data corresponded to the apoenzyme, as there was no electron density at the metal sites. We were able to identify two separate conformational states of the holo form, based on the data sets D153GX2 and D153GX4, as the reintroduction of metals into the apo crystals results in an extremely slow recovery (between 2 and 8 weeks) back to the original holo form (Dealwis et al., 1995). The two conformational states have been termed as structural intermediates I and II, as they represent the transformation of the apo form to the holo form in a slow, time-dependent manner. At the resolution of this

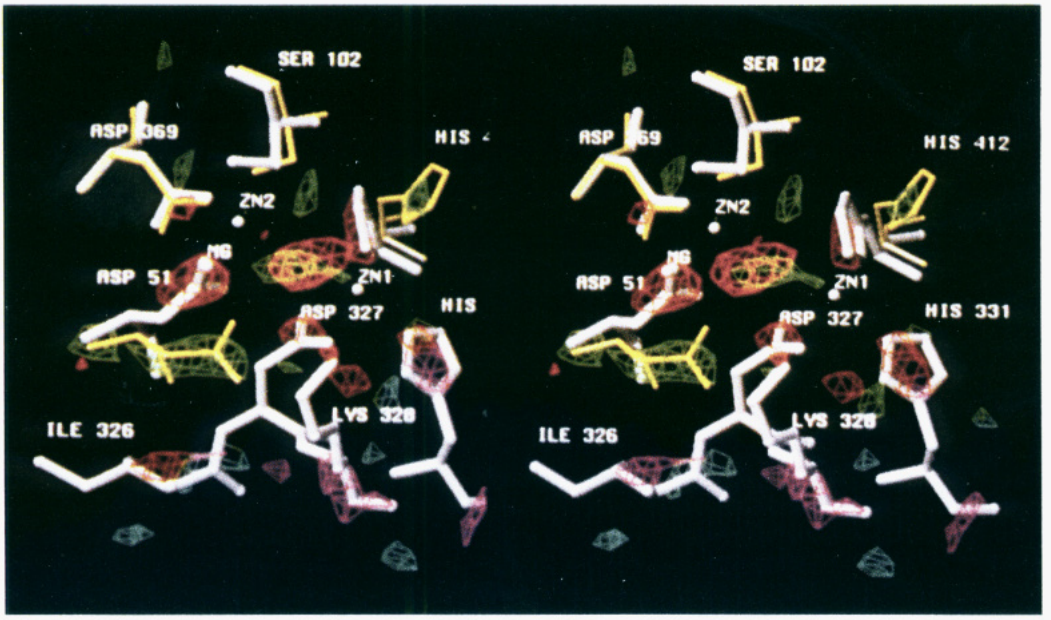

FIGURE 2: Stereoview of the $F_{apo} - F_{holo}$ difference Fourier electron density map calculated with the contribution of the three metal sites removed from the F_{holo} term. It illustrates the conformational change undergone by Asp 51 upon metal depletion. The red contours represent negative difference density (at -5σ) while the green contours depict the positive difference density (at $+5\sigma$). These peaks are the highest difference peaks in the entire map. The carboxyl side chain of Asp 51 moves from the negative density (red) in the holo form to the positive density (green) in the apo form. The holo structure (Dealwis et al., 1995) is represented by a thick white stick model while the apo structure is represented by a thin yellow stick model. Residues 324−331 have been omitted from the apo structure due to disorder.

Table 3: Pairwise Comparison of the Structural Intermediates of the D153G Mutant of AP[a]

	D153GNP (holo)	D153GDM (apo)	D153GX2 (int I)	D153GX4 (int II)
D153GNP (holo)		0.26 (429) 27.1%	0.21 (449) 19.1%	0.20 (449) 16.2%
D153GDM (apo)			0.25 (429) 16%	0.32 (429) 26.4%
D153GX2 (int I)				0.23 (449) 18.3%
D153GX4 (int II)				

[a] The top line in each cell is the RMS difference of the two AP subunits, based on a pairwise Cα superposition given in Å. The number of equivalent Cα pairs found within 2.5 Å is listed in parentheses. The bottom line of each cell shows the local *R*-factor, based on $\sum_{hkl}((|F_1| - |F_2|)/|F_1|)$ between data sets, after scaling them together. D153GNP, holo structure of the D153G mutant determined with data from fresh crystals (Dealwis et al., 1995). D153GDM, structure of the D153G mutant determined with data from the apo crystals. D153GX2, intermediate I structure of the D153G mutant determined with data from apo crystals after a 2 week soak of Mg^{2+} and Zn^{2+}. D153GX4, intermediate II structure of the D153G mutant determined with data from apo crystals after a 2 month soak of Mg^{2+} and Zn^{2+}.

crystallographic study, there seems to be no convincing evidence for a mixture of conformations present within each structure.

Evidence for time-dependent metal binding by this mutant is reflected by the values of the thermal parameters and relative occupancies at the three metal sites. The comparison of the temperature factors and relative electron density values of the Zn^{2+} and Mg^{2+} ions in the three refined metal-bound structures (Table 2a) shows that intermediate I has the lowest occupancy at all three metal sites. This is consistent with the intermediate I crystals being subjected to the shortest metal soaking period (2 weeks). In contrast, intermediate II has higher occupancies and lower *B*-factors at the three metal sites due to the metals being soaked for a longer period (2 months).

The results from the pairwise superposition of the four structures of the apo, holo (Dealwis et al., 1995), intermediate I, and intermediate II as well as their differences based on diffraction data are given in Table 3. These results suggest that the apoenzyme is closer to intermediate I than any of the other structures and intermediate II is closest to the holo structure solved using fresh mutant crystals (Dealwis et al., 1995). The fact that the intermediate I structure is the closest to the apo form is consistent with the shorter metal soaking period (2 weeks) associated with it. In contrast, intermediate II has had sufficient soaking time (2 months) to almost return to the holo state (Table 3).

Large conformational changes are observed in the apoenzyme compared to the holoenzyme. As AP is a homodimer, the conformational changes observed at the mutant active site are transmitted through to the dimer interface via Tyr 275 and His 276 (Figure 1). For example, the equivalent loop to the 406−410 loop from subunit 2 (906−910) is also disordered (Figures 2 and 3a). Since the quality of the crystals remains essentially unchanged, these loop perturbations are not sufficient to dissociate the dimer in the presence of the crystal packing forces nor to disrupt the crystal contacts appreciably.

The conformational alterations that occur at the mutant active site upon the loss of the metal ions can be rationalized by carefully examining the environment of the metal binding sites (Figures 2 and 4). It is reasonable to assume that the Mg^{2+} ion leaks out first, due to the weaker Mg^{2+} binding exhibited by this mutant (Dealwis et al., 1995). This possibly results in the destabilization of Asp 51, a residue known to coordinate both the Mg^{2+} and the Zn^{2+} ions found in the M3 and M2 sites, respectively (Figures 2 and 4). As a consequence of this, the Zn^{2+} binding at the M2 site is weakened and possibly results in its displacement. The position of the carboxyl side chain of Asp 51 in the apoenzyme appears to be shifted by about 3 Å away from

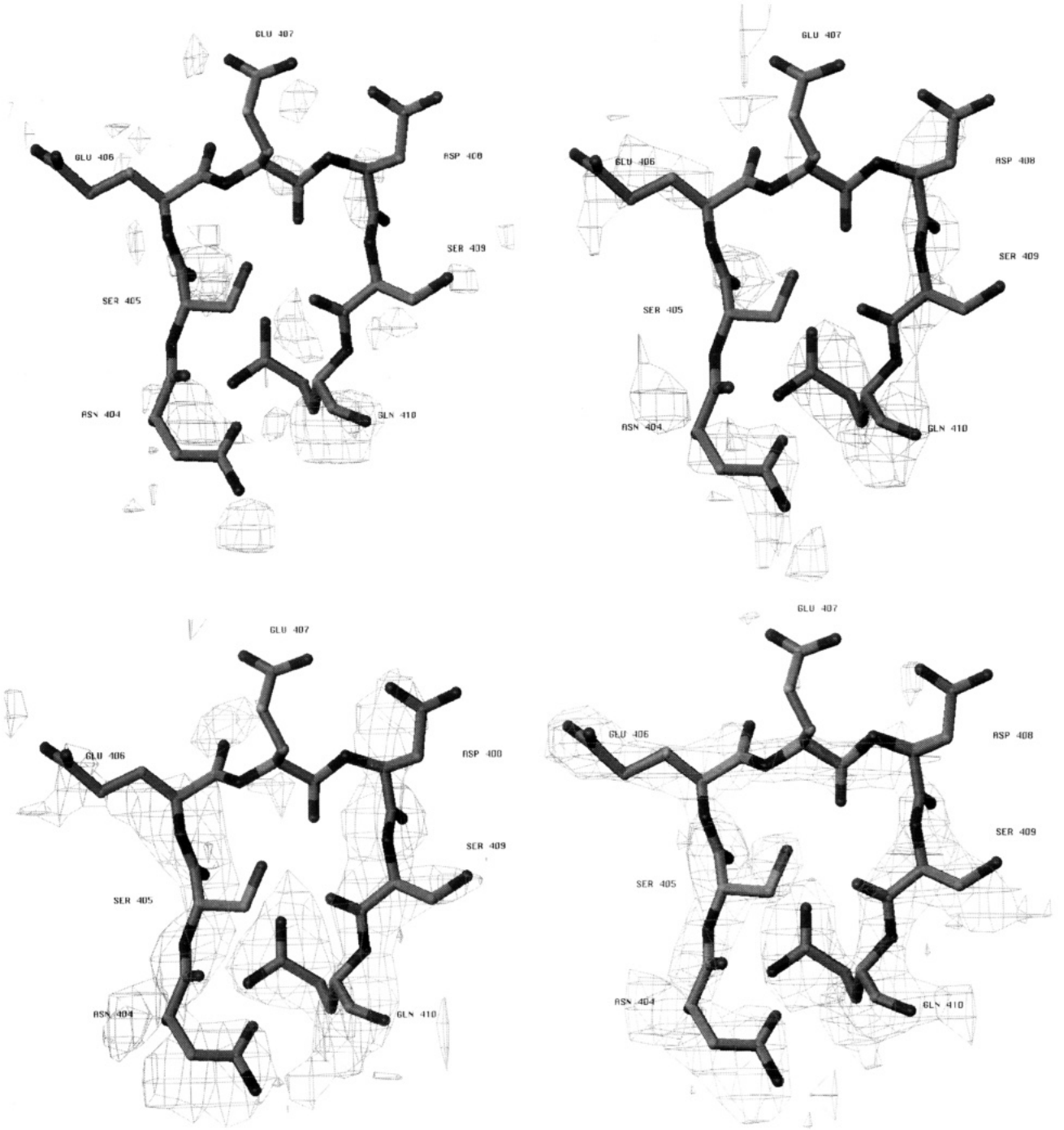

FIGURE 3: Progressive buildup of $2F_o - F_c$ omit maps from (a, top left) the apo enzyme, (b, top right) intermediate I, (c, bottom left) intermediate II, and (d, bottom right) the holo enzyme, in the region Asn 406 to Gln 410 contoured at 1.0σ. The molecular model used for display in all four figures is that of intermediate II after rigid-body refinement.

its position in the holoenzyme (Figure 2). This possibly results from the electrostatic repulsion between the two negatively charged aspartates, 51 and 369, occurring after the displacement of the Zn^{2+} ion, to which both of these side chains coordinate. The displaced side chain of Asp 51 sterically interferes with Asp 327 (Figure 2), resulting in the disruption of helix 324−331. In the refined apo structure, this helix was found to be disordered, as previously observed by Kim and Wyckoff (1991) in the AP wild type in the absence of metals. As the first zinc site at M1 is coordinated by the residues Asp 327 and His 331 within the helix, disordering of the helix destabilizes the M1 site (Figure 2) and weakens the binding of His 412 to the Zn^{2+} ion at the base of the disordered loop 406−410 (Figure 3a).

In the three-dimensional X-ray structure of intermediate I, the active site approaches an almost native-like conformation, except the side chains of Asp 51 and Asp 369 have altered conformations (Figure 4) and the water W454 which ligands the Mg^{2+} ion is probably not present (see metal• • • ligand distance in Table 2b). Although the helix 324−331 is fully ordered, the loop 407−410 is still partially disordered (Figure 3b). This may be partly due to the metal sites not being fully occupied. In contrast, the side chains of Asp 51 and Asp 369 return to a near native-like conformation in the intermediate II structure (Figure 4). The intermediate II structure is almost the same as the holo structure except for the absence of the active site solvent molecule W454 and the lack of main-chain electron density for residues 406−

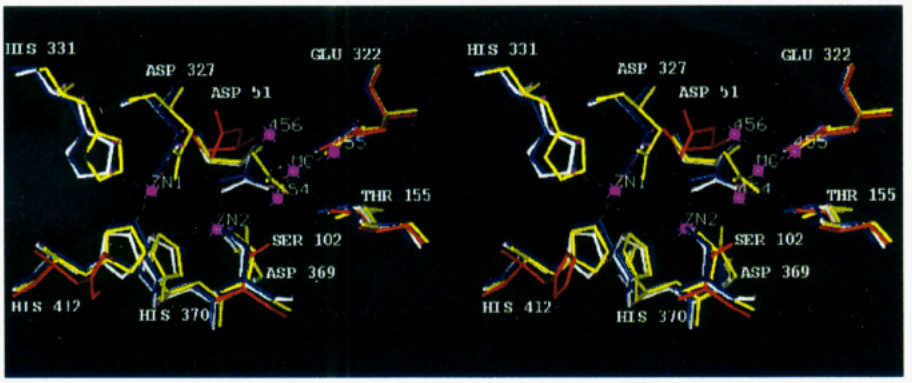

FIGURE 4: Superposition of the D153G mutant active site of the four structures. The apo form is drawn in red, intermediate I is drawn in yellow, intermediate II is drawn in blue, and the holo form based on data from fresh crystals is drawn in white. For simplicity, only the metal coordination of the holo form is shown. Residues 324−331 have been omitted from the apo structure due to disorder.

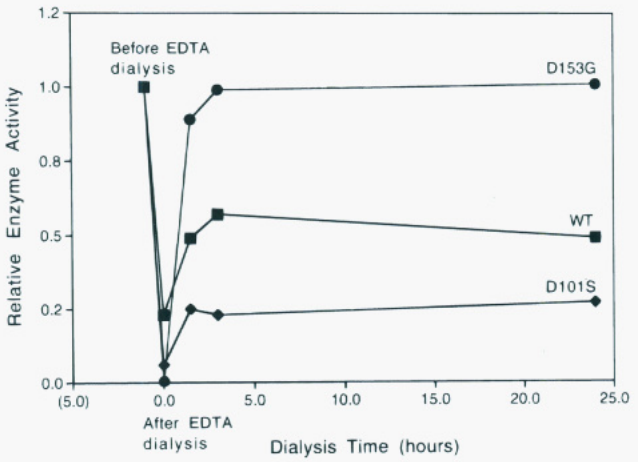

FIGURE 5: Removal and reintroduction of metals with the AP proteins in solution. The AP proteins were dialyzed in buffer containing EDTA (1 mM) to remove the metals. After dialysis in EDTA (24−48 h, 0 time point), the proteins were dialyzed in buffer containing 10 mM $MgCl_2$ and 1 mM $ZnCl_2$. Enzymatic activity was assayed before and after dialysis in the presence of metals as described in Materials and Methods and is expressed relative to the amount of activity present before dialysis in EDTA (−1 time point). The data points for wild-type AP (black squares, WT) and D153G (black circles, D153G) are the average of two independent experiments with each data point representing the mean of four activity assays. The data points for D101S (black rhombus, D101S) are from one experiment and are the average of two activity assays for each point.

408 of the surface loop (Figures 3c,d). In both of these intermediates, the guanidinium side chain of Arg 166, a residue involved in substrate binding (Kim & Wyckoff, 1991), has dual conformations, which is consistent with the flexibility thought to be exhibited by this residue (Dealwis et al., 1995).

Additional evidence for the reversible, time-dependent metal exchange in the D153G mutant protein was obtained from enzymatic studies (Figure 5) in solution. Upon dialysis in the presence of EDTA, D153G loses essentially all (>99%) of its activity, indicating that, as in the crystals of the protein, the Zn^{2+} and Mg^{2+} metals are not tightly bound and are readily removed. The D153G apoprotein recovers full activity when dialyzed in the presence of $ZnCl_2$ and $MgCl_2$, indicating that the metal-dependent conformational changes between the apo- and holoenzyme are completely reversible. In contrast, both the wild-type and D101S mutant proteins failed to demonstrate reversible metal binding (Figure 5). After dialysis in EDTA, both wild-type and D101S retain some enzymatic activity (23% and 6%, respectively). Furthermore, these enzymes show rapid but incomplete reactivation upon dialysis in the presence of metals. It is likely that for wild type and D101S the metals are not fully removed by EDTA due to the strength of metal−protein interactions. The rapid but incomplete reactivation upon addition of metals may represent the fraction of protein that has not lost all of its metals and is thus in a conformation that can still rebind them. The fraction of protein that has lost all metals may be irreversibly altered (denatured) so that it cannot rebind metals and be fully reactivated.

Previous biochemical work on the mutant D153H and the double mutant D153H/K328H suggested that these mutants undergo a time-dependent activation induced by the presence of Mg^{2+}, and that the process most probably involved a conformational change (Janeway et al., 1993). Although in a different mutant, our crystallographic results indirectly support the above conclusion. The fully reversible conformational changes occurring in the crystals of the D153G mutant of *E. coli* alkaline phosphatase upon metal depletion and reinsertion have been observed and analyzed. On the basis of these results the sequence of events involved in metal depletion can be explained as follows. The mutation of Asp 153 to glycine results in destabilizing the Mg^{2+} ion which slowly leaks out when left in a harvesting solution void of Mg^{2+} and Zn^{2+} ions. This, in turn, perturbs the environment of the Zn^{2+} ion in the M2 site, causing its displacement. These events lead to significant conformational changes being induced in a helix (324−331) and in the loop (404−412), which are both involved in binding the Zn^{2+} ion at the M1 site. As a consequence of this Zn^{2+} ion at the M1 site is possibly displaced. It is conceivable that the Mg^{2+}-induced activation observed in various enzyme mutants at the Asp 153 position (Asp153 → Ala, Matlin et al., 1992; Asp153 → His, Murphy et al., 1993) occurs by a cascade of events initiated by the binding of the divalent cation at the M3 metal site, which probably is a reversal of the steps outlined above.

Although the solution studies suggest a relatively fast (~5 h) elastic recovery of the full enzymatic activity (Figure 5), a longer time will be required for the metals to diffuse completely into the crystal lattice, making it difficult to assess the time scale of the complete structural recovery process. However, our crystallographic results suggest that in the D153G mutant of *E. coli* AP there are at least two or possibly more distinct structural intermediates with full enzymatic activity. It is conceivable that these intermediates correspond

(or are analogous) to the ones observed by Subramanian et al. (1995) in the refolding studies of native AP as monitored by phosphorescence of Trp 109.

In this study, we have observed how subtle, localized structural alterations taking place in the vicinity of the active site upon metal removal migrate to distant regions (>20 Å) of the macromolecular fold (Figure 1). In addition, due to the slow rate of the metal exchange process, we have been able to analyze the structural changes occurring upon metal recovery and to show that they are fully reversible in solution and in the crystalline state. These results could serve as a framework to simulate such a process by the methods of computational molecular dynamics and to further our understanding of the conformational changes observed in other metalloproteins upon metal depletion.

ACKNOWLEDGMENT

We thank Dr. J. Greer for critical reading of the manuscript and Drs. M. Klass and T. Perun for support. We are grateful to Prof. K. Moffat and Drs. V. Shrajer, K. Ng, V. Giranda, S. Muchmore, and C. Park for useful discussion. We appreciate the assistance of Jim Sukowski from Abbott's Creative Network in preparing the figures.

REFERENCES

Bartunik, H. (1983) *Nucl. Instrum. Methods 208*, 523−533.
Brennan, C., Christianson, K., Surowy, T., & Mandecki, W. (1994) *Protein Eng. 7*, 509−514.
Brünger, A. T., Kuriyan, J., & Karplus, M. (1987) *Science 235*, 458−460.
Brünger, A. T., Krukowski, A., & Erickson, J. E. (1989) *Acta Crystallogr., Sect. A 46*, 585−593.
Butler-Ransohoff, J. E., Kendall, D. A., & Kaiser, E. T. (1988) *Proc. Natl. Acad. Sci. U.S.A. 85*, 4276−4278.
Chaidaroglou, A., & Kantrowitz, E. R. (1989) *Protein Eng. 3*, 127−132.
Chaidaroglou, A., Brezinski, D. J., Middleton, S. A., & Kantrowitz, E. R. (1988) *Biochemistry 27*, 8338−8343.
Chen, L., Neidhart, D., Kohlbrenner, M., Mandecki, W., Bell, S., Sowadski, J., & Abad-Zapatero, C. (1992) *Protein Eng. 5*, 605−610.
Chlebowski, J. F., Armitage, I. M., & Coleman, J. E. (1977) *J. Biol. Chem. 252*, 7053−7061.
Coleman, J. E., & Gettings, P. (1983) *Adv. Enzymol. Relat. Areas Mol. Biol. 55*, 381−452.
Collaborative Computational Project, Number 4 (1994) The CCP4 Suite: Programs of Protein Crystallography, *Acta Crystallogr. D50*, 760−763.
Dealwis, C. G., Chen, L., Brennan, C., Mandecki, M., & Abad-Zapatero, C. (1995) *Protein Eng.* (in press).
Gosh, S. S., Bock, S. C., Rokita, S. E., & Kaiser, E. T. (1986) *Science 231*, 145−148.
Hajdu, J., Machin, P. A., Campbell, J. W., Greenhough, T. J., Clifton, I. J., Zurek, S., Gover, S., Johnson, L. N., & Elder, M. (1987) *Nature 329*, 178−181.
Hull, W. E., Halford, S. E., Gutfreund, H., & Sykes, B. D. (1976) *Biochemistry 15*, 1547−1561.
Janeway, C. M. L., Xu, X., Murphy, J. E., Chaidaroglou, A., & Kantrowitz, E. R. (1993) *Biochemistry 32*, 1601−1609.
Jones, T. A. (1978) *J. Appl. Crystallogr. 11*, 268−272.
Kim, E. E., & Wyckoff, H. (1991) *J. Mol. Biol. 218*, 449−464.
Luzzati, V. (1953) *Acta Crystallogr. 6*, 142.
Mandecki, W., Shallcross, M. A., Sowadski, J., & Tomazic-Allen, S. (1991) *Protein Eng. 4*, 801−804.
Matlin, A. R., Kendall, D. A., Carano, K. S., Banzon, J. A., Klecka, S. B., & Solomon, N. M. (1992) *Biochemistry 31*, 8196−8200.
Moffat, K., Bilderback, D., Schildkamp, W., & Volz, K. (1986) *Nucl. Instrum. Methods, Sect. A 246*, 627−635.
Moffat, K., Chen, Y., Ng, K., McRee, D., & Getzoff, E. D. (1992) *Philos. Trans. R. Soc. London, A 340*, 175−190.
Murphy, J. E., & Kantrowitz, E. R. (1994) *Mol. Microbiol. 12*, 351−357.
Murphy, J. E., Xu, X., & Kantrowitz, E. R. (1993) *J. Biol. Chem. 268*, 1−4.
Schlichting, I., Almo, S. C., Rapp, G., Wilson, K., Petratos, K., Lentfer, A., Wittinhoffer, A., Kabsch, W., Pai, E. E., Petsko, G. A., & Goody, R. S. (1990) *Nature 345*, 309−315.
Schlichting, I., Berendzen, J., Phillips, G. N., & Sweet, R. M. (1994) *Nature 371*, 808−812.
Schwartz, J. H. Crestfield, A. M., & Lipmann, F. (1963) *Proc. Natl. Acad. Sci. U.S.A. 49*, 722−729.
Sowadski, J. M., Handschumacher, M. D., Murphy, H. M. K., Kundrot, C., & Wyckoff, H. W. (1983) *J. Mol. Biol. 170*, 575−581.
Subramaniam, V., Bergenhem, N. C. H., Gafni, A., & Steel, D. G. (1995) *Biochemistry 34*, 1133−1136.
Teng, T.-Y., Srajer, V., & Moffat, K. (1994) *Nature Struct. Biol. 1*, 701−705.
Wilson, I. B., Dayan, J., & Cyr, K. (1964) *J. Biol. Chem. 239*, 4182−4185.
Xu, X., Qin, X.-Q., & Kantrowitz, E. R. (1994) *Biochemistry 33*, 2279−2284.

BI951421+